Quasicontinuous x-ray laser with λ = 10.8 nm in Pd-like tungsten using a nanostructured target

E. P. Ivanova

Institute of Spectroscopy, Russian Academy of Sciences, 142190 Troitsk, Moscow Region, Russian Federation

A new-generation x-ray laser project is explained. It is based on the transitions in Pd-like ions in nanoplasmas. The gain coefficient is calculated for the $4d^9_{3/2}5d_{3/2}[J = 0] - 4d^9_{3/2}5p_{1/2}[J = 1]$ transition ($\lambda \approx 10.8$ nm) in Pd-like tungsten. It is suggested that a cylindrical target made of nanostructured tungsten is pumped in the longitudinal direction by a laser pulse with energy 1–2 keV and duration $\sim$500 ps. For this pump pulse the target density and dimensions are calculated, as well as the temporal variations of the optimal plasma parameters for attaining $gL \sim 14$. The energy yield in the 10.8-nm line is more than 10^{20} eV.

PACS number(s): 42.55.Vc, 52.38.Ph

I. INTRODUCTION

Many applications require short-wavelength ($\lambda \sim$ 1–15 nm) x-ray lasers (XRL) with an energy yield $\gg$1 J and duration $\geqslant$1 ns. To design XRL, one needs pulsed IR pump lasers with a pulse energy >1 keV and duration $\sim$1 ns [1].

Recently a compact Nd-glass laser system with a pulse energy of $\sim$5 kJ and duration of about 1 ns has been developed in Germany (Darmstadt). Its peak intensity is 10^{21} W/cm^2 [2]. Higher-power but nevertheless compact laser systems have been developed at the National Ignition Facility (Livermore, CA, USA) [3].

XRL with a large energy yield and high conversion coefficient in the above-mentioned wavelength range can be developed on transitions in multiply charged ions in radiative-collisional scheme. An XRL project on transitions in Ne-like ions was proposed in Ref. [4]. The first experiments on observing spontaneous emission amplification in plasma were performed on transitions in Ne-like selenium [5]. Subsequent studies [6,7] proved that the Ni-like scheme is more efficient, because Ni-like ions (having the same laser transition wavelength as the Ne-like ones) can be ionized at a several times lower electron temperature. In addition, the optimal electron density and, correspondingly, the recombination loss in plasma in the Ni-like scheme are much less than in the Ne-like scheme. Note that the XRL with $\lambda = 13.9$ nm in Ni-like silver has been actively studied for 2 decades [8–12]. The laser based on Ni-like silver with $\lambda = 13.9$ nm is used in materials science, dense plasma diagnostics, ablation and holographic studies, and atomic physics. XRL based on Ne- and Ni-like schemes were reviewed in Ref. [13], where some directions in XRL applications were also outlined.

Beginning with the demonstration of the first XRL, the plasma formed as a result of interaction of pump radiation with a solid ($\leqslant$1-μm-thick foil) is used as an active medium in the overwhelming majority of experiments. In recent years some attempts have been made to increase the XRL energy yield using a metal target with a porous coating [14]. As the calculations [14] showed, this makes it possible to significantly increase the quantum yield of Ne-like copper XRL with $\lambda = $ 12.6–14.6 nm. The x-ray pulse FWHM was calculated to be $\sim$300 ps [14].

The past decade is characterized by progress in solving the main problems in XRL design: (i) decrease in overall dimensions; (ii) increase in the pump pulse energy; (iii) increase in the pulse-repetition frequency; (iv) improvement of the target quality (in order to increase the pump energy consumption); (v) increase in the plasma homogeneity (to reduce divergence and increase coherence of the output short-wavelength radiation); and (vi) increase in the focusing quality.

One of the most important problems is to optimize the 10- to 15-nm laser, for which a multilayer mirror with a high reflection coefficient has been designed [15–18]. XRL with energy $\leqslant$1 J within the carbon-oxygen window (the so-called water window of 2.3–4 nm) is very promising for medical applications and *in vitro* studies of biological structures (in particular, cells, proteins, molecules, etc.) with a high spatial resolution.

To date, the pump conversion coefficient into the short-wavelength energy in modern x-ray lasers is $\eta \sim 10^{-6}$; the maximum yield in the known laboratory systems reaches a few μJ per short-wavelength pulse [10]. Such a low conversion is caused by the following factors: (a) low pump energy consumption in the target because of reflection and scattering, (b) small volume of the active medium (the solid target expands during and after irradiation by a pump pulse and appropriate conditions for lasing are implemented in a $\sim$40- to 50-μm-thick plasma layer), (c) short amplification time (few tens of picoseconds), (d) the presence of debris in plasma leading to its degradation, and (e) spatial divergence of XRL radiation (caused by plasma inhomogeneity), which breaks its coherence.

II. JUSTIFICATION OF THE USE OF CLUSTER

To amplify spontaneous radiation with $\lambda = 10$–15 nm, the following parameters must be realized: optimal electron density $n_e^{\rm opt} \sim 10^{21}$–$10^{22}$ cm^{-3} and electron temperature $T_e \geqslant 1.5$ keV for the Ne-like scheme and $n_e^{\rm opt} > 10^{20}$ cm^{-3}, $T_e > 0.5$ keV for the Ni-like scheme. For both cases the recombination and bremsstrahlung losses in plasma at such a density are so high that one cannot maintain plasma in the optimal state in routine laboratory facilities. Generally amplification is observed using fairly short ($\leqslant$1 ps) pump pulses, which can provide sufficiently high T_e values; thus, the amplification occurs in the ionization mode: under optimal conditions an active ion over ionizes for few tens of picoseconds.

The experiments of the mid-1990s [19–22] showed that irradiation of a cluster target by an intense ultrashort laser pulse may produce a plasma with a temperature exceeding that of the plasma formed as a result of interaction of the same pulse with a gaseous or solid target by several orders of magnitude. Highly charged ions of noble gases with energies above 1 MeV and few-keV electrons were detected in Refs. [21,22]. The mechanisms of heating the plasma formed due to the exposure of a cluster jet to an intense laser beam (nanoplasma) were discussed in Refs. [23–25]. The interaction of the laser pulse optical field with a cluster leads to external ionization: escape of the generated photoelectrons from the cluster. Then the ionized cluster rapidly expands, and the electrons are heated to a temperature of few keV; this process is accompanied by electron-impact ionization. Focused pulsed laser beams transforms the material in the focus into relatively homogeneous plasma consisting of free electrons and multiply charged atomic ions. The charge composition, temperature, density, and radiation characteristics of this plasma depend strongly on the method of cluster beam formation, laser pulse parameters, the method of focusing, polarization and interaction conditions. As experiments [26,27] have shown, the above mechanism of xenon cluster ionization can be implemented if the laser intensity is no less than 10^{14} W/cm^2.

The independent experiments [26,27] on the interaction between the optical field of high-intensity laser pulse with a xenon cluster jet revealed an anomalously high quantum yield in the range of 10–15 nm. For $\lambda = 13.4 \pm 2.2$ nm the pump energy conversion coefficient into this line intensity was about 0.5% in 2π sr in both experiments. In Refs. [28,29] we developed a model of high-intensity monochromatic radiation source with $\lambda = 4$, 10, 11.3, and 13–13.9 nm on transitions in Ni-like xenon. The plasma was assumed to be formed as a result of interaction of xenon cluster jet with an ultrashort laser pulse. Within this model we determined the plasma filament density, temperature, diameter, and length; these parameters turned out to be in good agreement with the corresponding experimental data [26,27]. The energy yield at the wavelength in the range of 10–15 nm, calculated in Ref. [28], was also in good agreement with the experimental results. The time dependencies of the gain at different values of plasma parameters were determined for each transition.

High-energy consumption in a solid foam target was demonstrated in a number of experiments [1,30–33]. Laser radiation absorption and energy transfer in porous targets irradiated by a neodymium laser beam with an intensity of 10^{14} W/cm^2 and pulse duration of 2.5 ns were experimentally investigated in Refs. [1,30]. Methods for diagnostics of the plasma formed were developed in Refs. [1,30]. It was shown that dense high-temperature plasma efficiently absorbing laser radiation is formed in a porous target. The emission spectra of the plasma formed in a porous target irradiated by an Nd laser beam were analyzed in detail in Ref. [31]. The plasma electron and ion temperatures were determined from these measurements. The effect of the low-density foam (porous) target microstructure on the plasma parameters and the physical processes in the plasma were investigated in Ref. [32].

It is well known that the formation of homogeneous plasma is determined to a great extent by the laser pulse-
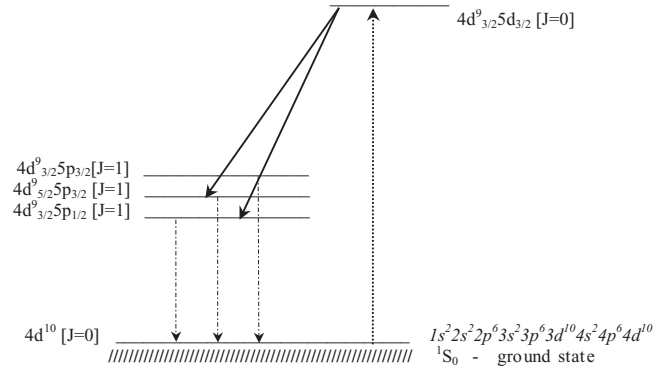
FIG. 1. Quasi-cw laser transitions in Pd-like tungsten.

target interaction time. In particular, nanosecond pump pulses can be used to generate highly homogeneous plasma. The calculations [34] and experiments [35] showed that the plasma homogeneity could be significantly improved using an axicon.

III. JUSTIFICATION OF THE USE OF THE PD-LIKE SCHEME FOR DEVELOPING A NEW GENERATION QUASICONTINUOUS XRL

The radiative-collisional XRL model uses closed-shell ions in the ground state. The laser-transition scheme for Pd-like tungsten is shown in Fig. 1.

An attempt to demonstrate lasing in Pd-like xenon (Xe IX, $\lambda = 41.8$ nm) in the plasma formed as a result of irradiation of a xenon cluster jet by a Ti-sapphire laser pulse (10 TW, 810 nm, 55 fs, 10 Hz) was made in Ref. [36]. Two types of valves were used to form a cluster flux: conical (with a round hole) and slitlike. The atomic density was varied in the range of $1.1 \times 10^{17} - 3.3 \times 10^{19}$ cm^{-3}, the xenon pressure in the chamber was changed from 0.013 to 4 MPa (0.13–40 atm), and the average cluster size was varied in the range of 15–50 nm. The laser radiation was focused into a region with a diameter $d \approx 25$ μm and a few millimeters long (for the slit valve the focusing was performed along the slot cluster jet). Two pumping techniques were investigated for both valve types: with and without irradiation by a preliminary pulse. The experiments showed *intense lasing for the case of* slot valve with a single pump pulse ($I_{pump} \sim 350$ mJ) (i.e., without a preliminary pulse). However, in Ref. [36] the attention was focused on the x-ray yield from a plasma formed using a preliminary pump pulse. The delay of the main (heating) pulse varied within 2–4.5 ns. The maximum energy of the output pulse with $\lambda = 41.8$ nm was 95 nJ (i.e., 2×10^{10} photons). This value exceeds the energy obtained in the experiment [37], where plasma was formed as a result of interaction between the laser optical field (with the same pump energy) and gaseous xenon in a capillary, by a factor of 2.5. Thus, the conversion coefficient obtained in Ref. [36] was $\sim 3 \times 10^{-7}$.

Note that the interaction of a 350-mJ pump pulse with a xenon cluster jet in a volume of $\sim 10^{-5} - 10^{-4}$ cm^3 leads to a very high electron temperature ($T_e \geqslant 10$ keV). Under these conditions the lifetime of the Xe IX ion in the plasma is less than 3 ps, because it is rapidly ionizing into the Xe X and higher ionization stages. As a result, the gL values sufficient for a high quantum yield cannot be obtained. At the same

time, the preliminary pump pulse causes a high radiation loss during the delay before the main pulse; this loss is related to the intrinsic plasma emission and heating of the adjacent cluster layers. Thus, the efficiency of this scheme does not exceed much that of the XRL based on the optical-field ionization of neutral atoms [37]. Note that in Ref. [36] the pump parameters were not optimized for the efficient use of the almost 100% energy consumption in the plasma upon pump field-cluster jet interaction. The laser pulse parameters and target density and geometry can be chosen so as to make plasma generate a coherent x-ray laser pulse with a high-energy yield. The problem of improving plasma homogeneity will be discussed below.

The purpose of this calculation is to find an active ion capable of generating (under optimal plasma conditions) an XRL pulse at least $\geqslant 500$ ps long and determine the nanostructured target parameters for this ion [atomic (electron) density n_i, (n_e), time dependence of electron temperature $T_e(t)$, target diameter d, and target length L] necessary for the maximum energy yield of amplified radiation in the range of 10–15 nm. The result obtained is a model experiment, which can be used to determine the pulse parameters and necessary pumping conditions.

In fact this problem is reduced to determining the plasma parameters at which the populations of active-ion levels are quasistationary; i.e., the ionization processes for an active ion are compensated by recombination processes. At the same time active-level inversion must provide a sufficiently high gain. We calculated such quasi-steady-state spectra for Ni-like xenon in Ref. [29]; they were experimentally observed in Ref. [38]. It is important that both the calculation and experiment gave the same values $T_e \approx 400$ eV and ionization balance [Xe XXVII] ≈ 0.4 for the plasma. At this electron temperature the lasing-transition inversion is too low to observe spontaneous-transition amplification. The time dependencies $g(t)$ for Ni-like xenon transitions in a long-pulse-pumped plasma were reported in Ref. [29].

We demonstrated the quasi–steady state of inverted active levels of Ne-like silver ions in a plasma with $T_e = 2$–3 keV, $n_e \geqslant 10^{21}$ cm^{-3}, and $d = 5$ μm, with dominance of these ions, in Ref. [39]. It was shown that the ionization balance is stable under these conditions; the gain value is also steady state and amounts to few tens of cm^{-1}. However, both for Ni-like xenon and for Ne-like silver ions it is fairly difficult to maintain plasma with so large n_e values using laboratory plasma sources, mainly because of very high recombination and bremsstrahlung losses.

One of the directions in XRL studies is the search for new schemes using low optimal n_i, n_e, values (ensuring low radiation loss) and high gains. The obvious way is the Pd-like XRL scheme, which was experimentally demonstrated for the first time in 1994 [$4d^9 5d\ ^1S_0$–$4d^9 5p\ ^1P_1$ transition with $\lambda = 41.8$ nm in Pd-like xenon (Xe IX)] [40]. The value $gL \approx 11$ (g is the gain and L is the active-medium length) was obtained in this scheme. Note that the Pd-like ion ground state is $1s^2 2s^2 2p^6 3s^2 3p^6 3d^{10} 4s^2 4p^6 4d^{10}$. The active medium was formed using the longitudinal scheme of gaseous xenon differentiated pumping with a cell length of 1–8 mm at a pressure of 12 torr. Pumping was performed by a circularly polarized laser beam with pulse duration of 40 fs, repetition

frequency of 10 Hz, and energy up to 70 mJ. The plasma diameter along the plasma filament length was not measured; based on the observed ion spectra the pump intensity along a length of 7.4 mm was found to be $I_{\text{pump}} \sim 3 \times 10^{16}$ W/cm^2. Another important pump characteristic is focus; a mirror with a focal length of 50 cm was used in Ref. [40]. The focal area, measured in air, was found to be 5×10^{-5} cm^{-5} along a length of ~ 1 cm. Based on these data the active plasma diameter was determined: $d \sim 100$ μm. Saturation along length L was not achieved in Ref. [40]. The results of Ref. [40] were basically confirmed by the experiments [37], where the value $gL = 15$ was reached at a xenon pressure of 15 torr and $L \approx 4$ mm. According to the results of Ref. [37], gain became saturated at this L value. The number of photons with $\lambda = 41.8$ nm, recorded by the spectrometer, was 5×10^9. The longitudinal scheme of gaseous xenon pumped by a circularly polarized 35-fs laser pulse with a repetition frequency of 10 Hz, intensity to 3×10^{17} W/cm^2, and maximum pulse energy of 330 mJ was used in Ref. [37]. These experiments were performed with a normal-incidence spherical mirror having a focal radius of 1000 mm and a resulting plasma diameter of 40 μm. In Ref. [41] we analyzed the plasma parameters in the experiments [37,40] and indicated the fundamental causes of different behavior of gain in the two experiments (electron temperature $T_e \leqslant 100$ eV and electron density $n_e = 3.4 \times 10^{18}$ cm^{-3} in Ref. [40] and $T_e \sim 200$ eV, $n_e = 4.2 \times 10^{18}$ cm^{-3} in Ref. [37]). Such low temperatures T_e are due to the large ionization cross sections of the electron shell with $n = 6$; they were calculated by us in Ref. [42].

However, the fundamental difference and advantage of the Pd-like XRL scheme is the relatively low electron density n_e^{opt} under optimal conditions. The necessary conditions for obtaining spontaneous amplification in the range of 10–15 nm are $n_e^{\text{opt}} \sim 10^{21}$–$10^{22}$ cm^{-3}, $T_e \geqslant 1.5$ keV for Ne-like ions and $n_e^{\text{opt}} > 10^{20}$ cm^{-3}, $T_e > 0.5$ keV for Ni-like ions. In both cases at such densities the recombination and bremsstrahlung radiation losses in the plasma are so high that the latter cannot be maintained in the optimal state in routine laboratory facilities. Generally amplification is observed when sufficiently short (<1 ps) pump pulses are used, which can produce rather large T_e values. Thus, amplification generally occurs when active ions fraction is diminishing due to ionization; the active ion lifetime is few tens of picoseconds.

In Ref. [43] we investigated the optimal conditions for XRL for seven Pd-like ions, from Er XXIII to Re XXX. It was shown that these ions have a high emission quantum yield with $\lambda = 10$–16 nm and $n_e^{\text{opt}} \approx (3$–5$) \times 10^{19}$ cm^{-3}. Omitting the general formulas for the bremsstrahlung and recombination radiation losses $dE/d\nu$ (see, for example, Ref. [44]), we will make a comparative estimation proceeding from the relation

$$dE/d\nu \sim n_e n_i Z, \tag{1}$$

where ν is frequency and Z is the ion charge. To provide lasing in the range of 10–16 nm in the Pd-like scheme, the product $n_e^{\text{opt}} n_i^{\text{opt}}$ must be two to three orders of magnitude smaller than for the Ni-like scheme. The low density leads to low radiation loss on intrinsic ion emission. This result indicates also that the optimal conditions can be maintained in a plasma

of relatively large volume and for fairly long times, using compact laboratory sources.

IV. THEORETICAL MODEL

The plasma formed as a result of the pump radiation–solid interaction is used as an active medium in the overwhelming majority of XRL experiments. Such experiments are generally preceded by a theoretical consideration, which can be divided into three computational problems:

(a) Calculation of the plasma expansion dynamics at specified external-source parameters. Magnetohydrodynamic calculations are generally performed in one- and two-dimensional approximations to determine the spatial and temporal distributions of the plasma density and temperature.

(b) Atomic-kinetic calculation of the active-ion level populations at specified plasma parameters and sizes. The radiation and electron-impact-induced transition rates (i.e., kinetic-equation coefficients) are calculated in the first stage. The electron-induced transition rates in the active ion depend on the plasma parameters. In the second stage the level populations and spontaneous amplification gains are determined by solving the kinetic equations.

(c) Calculation of the amplification dynamics for spontaneous radiation propagating in the plasma and of the XRL spatial coherence [45]. One of possible approaches is the solution of the Maxwell-Bloch equations [46,47].

For a nanostructured target with an atomic density corresponding to the optimal conditions for spontaneous-radiation amplification, it is not necessary to solve the first problem. Applying pumping with an appropriate energy and geometric optics, one can provide optimal conditions throughout the entire plasma volume. Note that for a sufficiently long XRL pulse ($t_{las} \geqslant 1$ ns) and small transverse sizes, one must take into account the plasma expansion, which reduces n_i, n_e at the plasma periphery, i.e., changes the refractive index along the radius. This causes output beam divergence and coherence violation. Some possible ways to solve this problem are discussed under Conclusions.

We do not calculate the XRL radiation propagation dynamics. Such calculations are generally performed to determine the gain saturation along the target length L. However, our analysis of numerous experiments showed that the spontaneous radiation is amplified when active ions are over ionizing; this circumstance imposes certain limitations on the target length. Generally the limit value is $gL \sim 14$–15 (this estimate was proposed in Ref. [48]), which corresponds to an increase in the radiation intensity I_0 by a factor of more than 10^6, where I_0 is the transition emission power from the active plasma volume into the spherical angle 2π.

The atomic-kinetic calculation is performed assuming plasma homogeneity; in this case, the following five parameters are sufficient for the calculation: electron and ionic densities n_e, n_i, temperatures T_e, T_i, and the plasma filament diameter d. To calculate the gain g at the line center we will use the known expression (see, for example, Ref. [49]):

$$g = A_{ul}\lambda^2[N_{up} - (g_u/g_l)N_{low}]/8\pi\,\Delta\nu_0, \qquad (2)$$

where A_{ul} is the probability of radiative transition between the upper (u) and lower (l) levels; λ is the transition wavelength;

$N_{up} = n_i P_{up}$ and $N_{low} = n_i P_{low}$ are the concentrations of ions in the upper and lower active states, respectively; P_{up} and P_{low} are the upper- and lower-level populations, respectively; and g_{up} и g_{low} are the statistical weights of the upper and lower levels, respectively. The transition line profile is determined by the convolution of the Doppler and natural profiles. The latter is due to the radiation transitions and collisional processes, which relate each level to all other levels of the W XXIX ion and to the ion in the adjacent ionization stage. $\Delta\nu_0$ is the line width at the center (Voigt profile); it is determined by the simplified method proposed in Ref. [49].

The atomic-kinetic calculation of the level populations and plasma charge composition was performed on the assumption that ions in two adjacent ionization stages dominate in the plasma. The ions in one of these stages are active (in our case W XXIX, for which 75 lower energy levels are taken into account in the kinetics). The typical inversion value is 5–20% of the upper level population. Thus, the inversion can be adequately estimated only when the level populations are calculated with high accuracy. This is provided by good accuracy of the rate coefficients in the kinetic equations, i.e., of the probabilities of the radiative and electron-impact-induced transitions. The kinetics also takes into account the states of the ion in the adjacent (previous) ionization stage: a set of Rydberg levels of this ion with $\zeta = 27$ corresponds to each level of the active ion with the charge $\zeta = 28$ (28 is the number of removed electrons). To reduce the number of kinetic equations, these levels are combined into three bands. The method for calculating the kinetics of level populations in two adjacent ions was described in Ref. [50]; the system of equations for the populations P_i of the active ion with the charge ζ and the populations P_j of the band of the adjacent ion with the charge $\zeta - 1$ can be written as

$$dP_i{}^\zeta/dt = \sum_{i'} C_{ii'}{}^{\zeta,\zeta}P_{i'} + \sum_j C_{ij}{}^{\zeta,\zeta-1}P_j$$

$$dP_j{}^{\zeta-1}/dt = \sum_{j'} C_{ij}{}^{\zeta-1,\zeta-1}P_{j'}, \qquad (3)$$

where $C_{ii'}$ are the coefficients relating the transitions between the levels of the active W XXIX ion (they are calculated within the quantum-electrodynamics approach with a satisfactory accuracy); C_{ij} are the coefficients relating the transitions between the active-ion levels and the Rydberg bands of the adjacent ion (W XXVIII); and $C_{jj'}$ are the coefficients relating the transitions between the bands of the adjacent ion. The coefficients C_{ij} and $C_{jj'}$ were calculated in the quasiclassical approximation using the formulas from Ref. [50]. The kinetics takes into account all basic processes involving two ions of adjacent ionization stages: dielectronic electron capture to the ground level of the active ion and its subsequent autoionization decay, due to which the active ion remains excited; as a result, the electron-impact excitation threshold for the active ion decreases. For the ion with the charge $\zeta - 1$ the electron-impact ionization, triple recombination, radiative and collisional transitions between Rydberg bands, and photorecombination are taken into account.

x-ray lasing occurs in optically dense plasma, where radiation reabsorption (trapping) is of fundamental importance; in sufficiently dense plasma the inversion disappears due to

the decrease in the lower active level depletion rate. The radiation reabsorption in plasma is taken into account within the Biberman-Holstein approximation via the escape factor G, which is the ratio of the effective radiative-transition rate $A_{\text{ul}}^{\text{eff}}$ for an ion in the plasma to the radiative decay rate A_{ul} for an isolated atom:

$$A_{\text{ul}}^{\text{eff}} = G A_{\text{ul}} \qquad (4)$$

The following formula was proposed in Ref. [51] to calculate the escape factor G for optically dense cylindrical plasma:

$$G = 1.22[\ln(k_0 d)]^{1/2}/(k_0 d), \qquad (5)$$

where k_0 is the absorption coefficient on a specified transition and d is the plasma column diameter.

The level populations were calculated by solving a system of many differential equations, with several tens of thousands of coefficients. The coefficients for different processes differ by several orders of magnitude. Note that not only strong transitions but also weaker ones are important in the calculations of the gains for long-pulse XRL. A detailed comparison of the electron-impact transition rates was performed in Ref. [52] by the example of Ne-like silver and Ni-like gadolinium. Generally the probabilities of strong transitions between active-ion levels ($C_{ii'}$), obtained in different theoretical calculations, are in good agreement. The coefficients $C_{ii'}$ for weak transitions might differ several times, depending on the calculation method used.

Correct population values at asymptotically large times can be determined by solving differential equations only in combination with some iteration method. To this end the system of differential equations is solved on certain (sufficiently small) iteration steps Δt_k. At the end of each step, the calculated level populations P_i, P_j, and new T_e values are used to calculate the distributions in the energy bands and the new coefficients of the differential equations. If the levels of an ion with $\zeta - 1$ are occupied at specified plasma parameters and the instant $t = 0$, one can estimate (by solving the kinetic equations) the time $\tau(T_e, n_e)$ necessary to transform the ion with $\zeta - 1$ into the state with ζ and the ionization balance within the approximation of two adjacent ions. We performed such investigations for Ne-like silver [39] and for Ni-like xenon [29] and established τ dependence on plasma parameters T_e, n_e.

V. ENERGY LEVELS AND TRANSITION PROBABILITIES FOR PD-LIKE TUNGSTEN

Ne-, Ni-, and Pd-like ions have a common property: their ground state is a closed electron shell. The energy levels and radiative transition probabilities for Ne- and Ni-like isoelectronic sequences were studied in detail up to $Z = 92$; the data obtained facilitate simulation of the emission spectra and search for optimal plasma conditions for XRL design.

There are hardly any spectroscopic data in the literature for Pd-like ions with $Z > 60$. The experimental energy levels in the lower $4d^9 4f$, $4d^9 5l$ ($l = 0$–4) configurations of relatively light Pd-like ions up to Nd xv ($Z \leqslant 60$) were reported in Refs. [53–59] (see also references therein). Within conventional experimental approaches it is difficult to identify the spectra of heavier Pd-like ions because of

the intense recombination and bremsstrahlung background. The experimental energy levels of heavy Pd-like ions up to Bi XXXVIII ($Z \leqslant 83$) are presented by two resonant transitions in the ground state: $4d^{10}$–$4d^9 4f\,^3 D_1, ^1 P_1$ in the only experimental work [60]. These data are insufficient to reproduce the entire Pd-like ion spectrum using the conventional approaches based on the multiconfiguration Dirac-Fock code.

We calculated the energy levels in Pd-like ions with $50 \leqslant Z \leqslant 83$ using the relativistic perturbation theory with model potential of zero approximation (RPTMP), which has been developed at the Institute of Spectroscopy, Russian Academy of Sciences, during the past 40 years. The RPTMP method was described in Refs. [61–63]. The formulas for calculating the energy levels of atomic systems with a closed electron shell in the ground state were reported in Refs. [64,65]. The formulas for the cross sections of electron-impact induced transitions in the above-mentioned atomic systems were derived in Ref. [66]. The theoretical approach to the calculation of radiative transition probabilities was presented in Refs. [67–69]. Within the relativistic perturbation theory the excitation energy of a Pd-like ion can be expanded in a series:

$$
\begin{aligned}
E(nl_1 j_1, n_2 l_2 j_2 [J M_J]) = {} & E^{(0)}_{\text{el}}(n_1 l_1 j_1) + E^{(0)}_{\text{vac}}(n_2 l_2 j_2) \\
& + \Delta E^{(2)} + \Delta E^{(4)} + \cdots, \quad (6)
\end{aligned}
$$

where $E^{(0)}_{\text{el}}(n_1 l_1 j_1)$, $E^{(0)}_{\text{vac}}(n_2 l_2 j_2)$ are the energies of one electron over the core and one core vacancy, respectively. In Ref. [64] the method for calculating $\Delta E^{(2)}$ was described, and the way to take into account the higher orders $\Delta E^{(4)}$ was introduced.

In the RPTMP method the functions of the states of one electron over the core and one core vacancy are determined by solving the Dirac equation with a zero-order model potential $V(r/b)$. The only parameter $b(nlj/Z)$ depends on the state nlj and nuclear charge Z; it is calculated by solving the Dirac equation with the known energy of one electron over the core (Cauchy problem). While the quasiparticle (electron/vacancy) binding energy rapidly changes along the isoelectronic sequence (leading term $\sim Z^4$); the parameter $b(nlj/Z)$ is a slowly varying function of Z. The reason is that the Dirac equation takes into account the overwhelming majority of Coulomb and relativistic interactions. As a result, the parameter $b(nlj/Z)$ is a convenient object for extrapolating over Z. Note that the exact values of $E^{(0)}_{\text{el}}(n_1 l_1 j_1) + E^{(0)}_{\text{vac}}(n_2 l_2 j_2)$ for all levels are 90–95% of the total energy $E(n_1 l_1 j_1, n_2 l_2 j_2 [J M_J])$, because they include the overwhelming majority of relativistic and correlation energies for the states of one electron over the core or one core vacancy. Another very important property of the RPTMP approach is the high asymptotic accuracy of the wave functions of one electron or one vacancy. This is essential when the integrals of the products of electron (or vacancy) wave functions and the functions of free-electron states are calculated. Such integrals are calculated to determine the cross sections of the electron-impact-induced transitions in the active ion.

The wavelengths of the resonant transitions to the ground state, $4d^{10}$–$4d^9 5p\,^3 P_1, ^1 P_1, ^3 D_1$; $4d^9 4f\,^3 P_1, ^3 D_1, ^1 P_1$; $4d^9 5f\,^3 P_1, ^3 D_1, ^1 P_1$, in Pd-like ions were reported by us in Refs. [70,71]. A comparison with the experimental results [53–60] indicates a good accuracy of the calculated energies.

TABLE I. Spectroscopic data for the lasing transitions in W XXIX shown in Fig. 1.[a]

Upper level	J	Lower level	J	λ (nm)	E_{tr} (eV)	A_{J0} (s^{-1})	A_{ul} (s^{-1})	R_{col} (cm^{-3} s^{-1}) $T_e = 300$ eV	R_{col} (cm^{-3} s^{-1}) $T_e = 500$ eV	R_{col} (cm^{-3} s^{-1}) $T_e = 900$ eV
$4d^9_{3/2}5d_{3/2}$[a]	0					0.0		2.8×10^{-10}	4.6×10^{-10}	5.8×10^{-10}
		$4d^9_{3/2}5p_{1/2}$	1	10.78	115	7.3×10^{11}	1.1×10^{11}	2.2×10^{-11}	3.0×10^{-11}	3.4×10^{-11}
		$4d^9_{5/2}5p_{3/2}$	1	12.08	103	1.2×10^{12}	6.5×10^{10}	2.7×10^{-11}	3.8×10^{-11}	4.3×10^{-11}
		$4d^9_{3/2}5p_{3/2}$	1	14.10	88	1.7×10^{11}	1.2×10^{10}	3.4×10^{-12}	5.0×10^{-12}	5.7×10^{-12}

[a]Wavelengths λ, transition energies E_{tr}, and radiative transition probabilities: A_{J0}, to the ground state $^1S_0$; A_{ul}, from the upper to the low active level. The rate of electron-impact excitation from the ground state per unit volume R_{col} is given for three electron temperatures.

The calculated spectroscopic constants and XRL characteristics for the $4d^{10}5d$ [$J = 0$]–$4d^{10}5p$ [$J = 1$] transition in the ions from Er XXIII to Re XXX were presented by us in Ref. [43]. The calculated transition wavelengths for these ions are in the range of 10–15 nm. The gains for the Pd-like Er XXIII–Re XXX ions were investigated in Ref. [43] for an ultra short pump pulse. This preliminary study showed that the gain nonmonotonically changes along Z. According to our calculations [43], the largest gains can be obtained for Yb XXV, Hf XXVII, and W XXIX.

Figure 1 shows two high-gain transitions from upper active level $4d^9_{3/2}5d_{3/2}$ [$J = 0$] to the low $4d^9_{3/2}5p_{1/2}$ [$J = 1$] and $4d^9_{5/2}5p_{3/2}$ [$J = 1$] levels and one weaker transition from this upper level to $4d^9_{3/2}5p_{3/2}$. The spectroscopic characteristics of the laser transitions in W XXIX, which can implement spontaneous emission amplification under a long pump pulse, are listed in Table I.

VI. OPTIMAL PLASMA PARAMETERS, SIZE, GAIN, AND CONVERSION COEFFICIENT

Under saturation conditions L may amount to few centimeters. Taking into account the plasma homogeneity, we will average $g(t)$ over the spatial and temporal coordinates. To this end, we divide the target into thin layers of thickness $\delta L(\delta L$ is much smaller than the pump-pulse spatial scale). In each layer elementary processes occur identically but with some delay in time. Then it is sufficient to average the function $g(t)$ over time. In each layer $I_{pump} \sim 10^{14}$ W/cm^2; thus, plasma is formed from tungsten clusters according to the overbarrier mechanism of cluster ionization, which was analyzed in detail in numerous experimental and theoretical studies [20–25]. The experiments with foam solid targets suggest that at such pump intensities the pump energy consumption in them can be as high as $\sim$50%.

Our calculation [43] for an ultrashort pump pulse interacting with a flux of tungsten clusters gave $n_e^{opt} = 7 \times 10^{19}$ cm^{-3} for $T_e = 500$–1000 eV. A strong dependence of the output laser pulse duration on the parameters n_e, T_e was observed.

In this calculation we first determine the optimal parameters n_e, T_e providing the longest lasing time with a sufficiently large asymptotic value of $g(t)$. These parameters will be found on the assumption that homogeneous plasma is formed instantaneously. After calculating $g(t)$ for the set of parameters n_e, T_e we obtain $n_e^{opt} = (2$–$4) \times 10^{19}$ cm^{-3}. Figures 2(a) and 2(b) show the dependences $g(t)$ for different values of T_e at $n_e = 2 \times 10^{19}$ and 4×10^{19} cm^{-3}. It follows from Fig. 2 that

at $T_e = 200$ eV the asymptotic values of $g(t)$ are too small to provide noticeable lasing. The optimal temperatures are in range $300 < T_e < 800$ eV. At $T_e > 800$ eV the amplification decays due to the very fast transformation of W XXIX into W XXX and subsequent ionization stages.

Due to the reabsorption effect the plasma diameter plays an important role in the calculations of $g(t)$, because at sufficiently large d the depletion rate of the lower active levels decreases, thus reducing the inversion. The decrease in $g(t)$
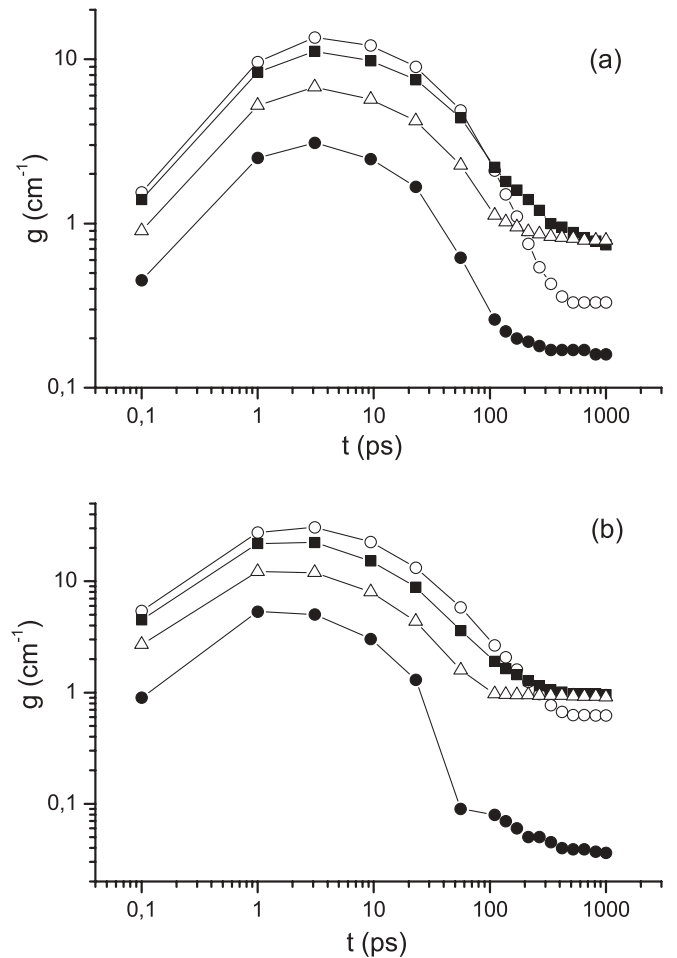
FIG. 2. Time evolution of the gain $g(t)$ for the $4d^9_{3/2}5d_{3/2}[J = 0]$–$4d^9_{3/2}5p_{1/2}[J = 1]$ transition ($\lambda = 10.78$) in W XXIX at $d = 100$ μm for $n_e = 2 \times 10^{19}$ cm^{-3}; (a), $n_e = 4 \times 10^{19}$ cm^{-3}; (b) $T_e = 200$ ($\bullet$), 300 ($\triangle$), 500 ($\blacksquare$), and 900 ($\circ$) eV. It is assumed that plasma is formed at $t = 0$.

(a)

(b)
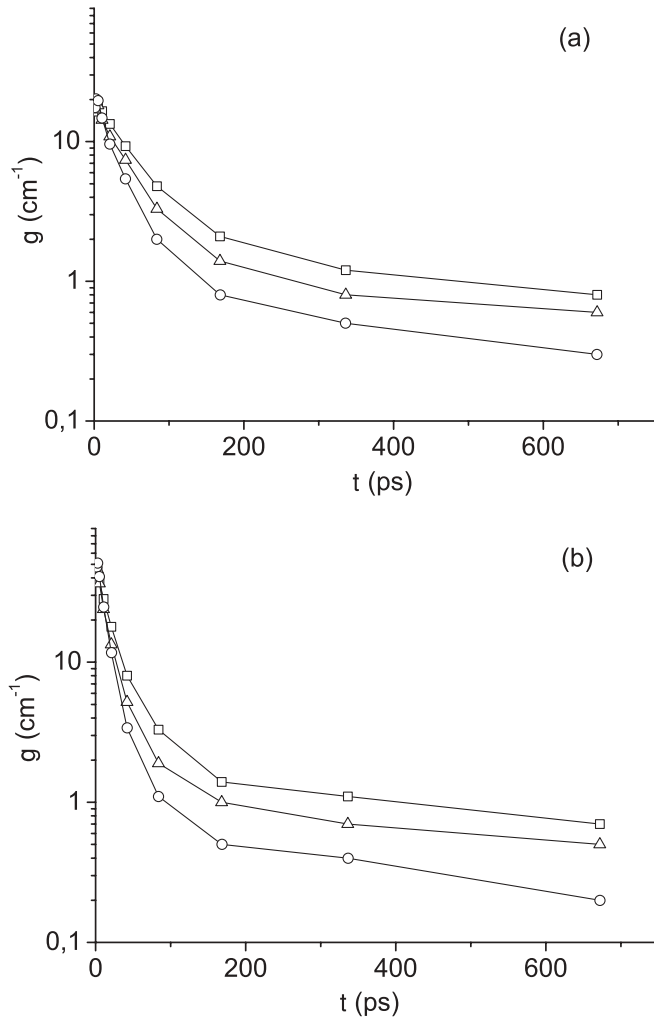
FIG. 3. Time evolution of the gain $g(t)$ assuming that plasma is formed at $t = 0$ with $T_e = 800$ eV and different plasma diameters: $d = 0.02$ ($\square$), 0.1 ($\triangle$), 0.5 ($\circ$) cm; $n_e = 2 \times 10^{19}$ cm^{-3}, (a) $n_e = 4 \times 10^{19}$ cm^{-3} (b).

with an increase in the plasma diameter is shown in Fig. 3. We assume the condition $d \leqslant 1$ mm to be satisfied for long laser pulses in W XXIX ions.

The calculation is performed for pumping by a standard 500-ps Nd YAG laser with pulse energy of about 1–2 kJ. The target is solid foam (nanostuctured) tungsten with an atomic density of 10^{18} cm^{-3} and has a cylindrical shape (1 mm in diameter). The pump radiation is focused using an axicon, which acts as a waveguide for the Ne YAG laser beam along the target axis.

The pump pulse shape is of fundamental importance. In particular, it was established in [72] that a pedestal pulse preceding the main (heating) pulse significantly increases the XRL duration and quantum yield. Here, we assume that the pump pulse has a high contrast and step profile, which can be divided into the preceding and main parts. It is shown in Fig. 4 by a dotted line. The preceding part is almost completely absorbed by the nanostructured target and provides plasma formation with $T_e \sim 200$–250 eV. According to our estimates, at this temperature the Pd-like tungsten stage is reached $\sim$300 ps after the pulse onset. Then the main part
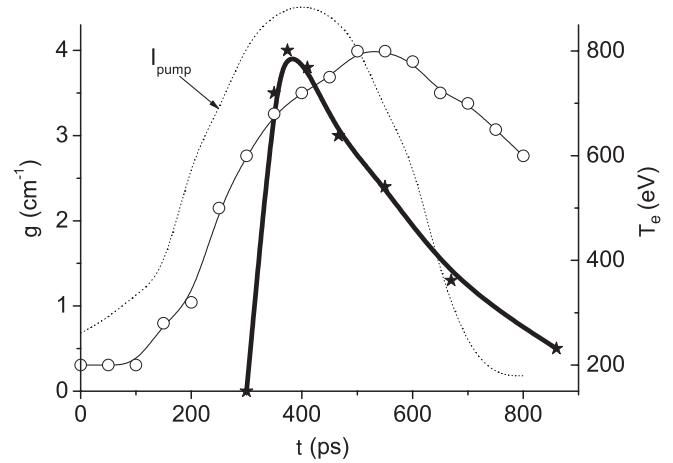
FIG. 4. Time evolution of the gain $g(t)$ assuming the real pump pulse with FWHM $= 500$ ps and energy $\geqslant 1$ keV. The pump pulse profile is shown with a dashed line in arbitrary units. T_e values are plotted on the right vertical axis (line $\circ$). $d = 0.1$ cm, $n_e = 3 \times 10^{19}$ cm^{-3}.

heats the plasma to $T_e \approx 600$–800 eV. The optimal function $T_e(t)$ is shown in Fig. 4 (right ordinate axis). During the interval $t = 300$–400 ps the gain $g(t)$ increases to maximum ($\sim$4 cm^{-1}). The subsequent decrease in $g(t)$ is caused by the following two factors: (i) reduction of the inversion as a result of electron-impact-induced mixing of level populations and (ii) transformation of W XXIX into W XXX and higher ionization stages.

The model calculation of $g(t)$ with the optimal n_e, $T_e(t)$, and $d = 1$ mm is shown in Fig. 4. Averaging on the intervals $t = 300$–600 and 300–800 ps yields $\tilde{g}(t)$ values of $\sim$2.8 and $\sim$1 cm^{-1}, respectively. Table II contains the Voigt widths $\Delta\tilde{\nu}$, averaged on a time interval of 300 ps, and populations of the upper and lower active levels $\tilde{N}_u$, $\tilde{N}_l$, and the output intensities I_0 per unit volume. The calculations were performed for $d = 1$ mm and $n_e = 3 \times 10^{19}$ cm^{-3}. The output lasing energy $E^{out}{}_{las}$ (eV) $\approx 1.5 \times 10^{20}$ eV from the plasma into a cross section with $d = 1$ mm was calculated for a target of length $L = 5$ cm. The model emission spectrum of W XXIX (with allowance for amplification at optimum) is shown in Fig. 5.

VII. JUSTIFICATION OF THE USE OF A CONICAL MIRROR (AXICON) AS A PLASMA WAVEGUIDE

The length of gain region for longitudinally pumped target x-ray lasers is severely limited by ionization-induced refraction. By using a waveguide to maintain sufficient pump intensity over a long distance, the length of gain region for the x-ray lasing can be increased and the size of the underionized absorptive region can be reduced.

A laser-produced plasma channel was shown [34] to be a promising means to produce an efficient x-ray laser, in which pump pulse and x-ray refraction away from the gain volume is eliminated. The channel provides a route for efficient high-power laser pumping through optical waveguiding of the pump. The channel also acts as a controllable waveguide for generated soft x rays as well as for the pump pulse, since it

TABLE II. Time averaged over the interval 300–600 ps values for the Voigt line width $\Delta\nu$, level populations N_u, N_l, and the gain g, calculated for $n_e = 3 \times 10^{19}$ cm^{-3}, T_e as in Fig. 4, and $d = 1$ mm. I_0 is the transition emissive power from unit volume, $E^{\text{out}}_{\text{las}}$ is the energy yield including the enhancement from the volume $V = \pi \times (0.05)^2 \times 5$ cm$^3 \approx 0.04$ cm^3.

Upper level	J	Lower level	J	λ (nm)	$\Delta\tilde{\nu}$ (10^{12} s^{-1})	$\tilde{N}_u$ (10^{15})	$\tilde{N}_l$ (10^{15} cm^{-3})	$\tilde{I}_0$ (10^{28} eV cm^{-3}/s)	$\tilde{g}$ (cm^{-1})	$E^{\text{out}}_{\text{las}}$ eV
$4d^9_{3/2}\,5d_{3/2}$	0					1.6				
		$4d^9_{3/2}\,5p_{1/2}$	1	10.78	1.2		2.1	2.2	2.8	1.5×10^{20}
		$4d^9_{5/2}\,5p_{3/2}$	1	12.08	1.4		2.1	1.2	1.4	1.3×10^{18}
		$4d^9_{3/2}\,5p_{3/2}$	1	14.10	0.9		1.8	0.2	0.6	2.6×10^{16}

has wavelength-independent mode. As a result, it is possible to produce a transversely coherent output amplified x-ray radiation.

The reflective axicon scheme is well suited for all applications that require both low dispersion and high conversion efficiency from Gaussian to Bessel beams such as waveguide production and nonlinear processes with laser pumping. Bessel beams are characterized by a transverse field profile defined by the zero-order Bessel function of the first kind. They exhibit several remarkable properties, such as diffraction-free propagation of the central peak over a distance fixed only by the geometry of the source device and superluminal phase and group velocities in free space.

The experiment [73] has spatially and temporally characterized an optical Bessel beam produced using a conical mirror propagating in free space. It was ascertained that the beam had a constant peak size over the propagation distance determined by the properties of the conical mirror. The diffractive-free region is limited by the finite extent of the beam. The maximum diffraction free propagation distance depends on radius R of the optical element used for producing the beam and on the axicon angle θ and is given by $z_{\max} = R/\tan\theta$. In Ref. [73] 65% of the Gaussian beam power was converted into a nondiffractive beam. The conversion efficiency is limited by the size of the Gaussian beam incident on the conical mirror that had 32% of its power outside the mirror area. Losses at the beam

splitter and the conical mirror are ∼3%. The radial intensity profile recorded at different distances is shown in Fig. 2 of the experiment [34]: they are almost identical over the entire diffraction-free region with a central peak.

In principal, the use of axicon can provide a plasma filament with high uniformity density profile. It was proved in the experiment [35] where dramatic enhancement of optical field ionization collisional-excitation x-ray lasing was achieved by using an optically preformed plasma waveguide. With 9-mm-long pure krypton plasma waveguide prepared by using the axicon-ignitor-heater scheme, the yield at 32.8 nm in Kr IX was enhanced by 400 folds relative to the case without plasma waveguide.

VIII. CONCLUSION

In the first XRL experiments [5] the pump energy conversion coefficient into the XRL energy was $\eta = 10^{-9}$–10^{-8}. Recent experiments with solid targets (foils) gave $\eta = 10^{-6}$–10^{-5} [8–12]. Modern XRL are generally characterized by the pulse duration τ_{las} of few tens of picoseconds. The following three factors can radically affect the further XRL study (by increasing the η и τ_{las} values) and stimulate new-generation XRL design.

(i) The use of the Pd-like scheme allows one to solve the problem of recombination and bremsstrahlung energy losses in plasma. For example, for W XXIX under optimal conditions, $n_e^{\text{opt}} \sim (2\text{--}4) \times 10^{19}$ cm^{-3}, $n_i \sim 10^{18}$ cm^{-3}; in this case, these losses are much smaller than that on the natural W XXIX ion emission in plasmas.

(ii) The use of nanostructured (nanoporous, solid foam) targets, for which the energy consumption exceeds that in solid or gaseous targets by at least three orders of magnitude. The main conditions are sufficiently high pump intensity ($I_{\text{pump}} \geqslant 10^{14}$ W/cm^2) and correctly chosen step profile of the pump pulse.

(iii) The use of a waveguide of axicon type for the pump beam, which provides a high degree of plasma homogeneity. Methods for calculating axicons of different type are intensively developed. These three factors form the basis of new-generation XRL with a conversion coefficient of ∼1% per line under consideration. Preliminary calculations of the target parameters, time characteristics, and conversion coefficients are also important for implementing this approach. Sufficiently accurate calculations will save time and labor when performing targets.
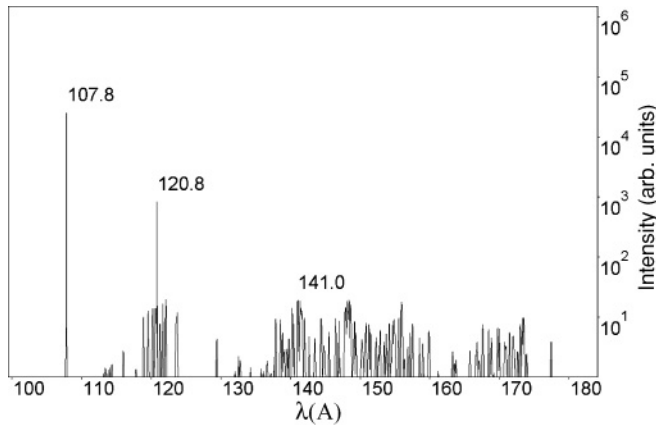
FIG. 5. Model W XXIX spectra with accounting for the enhancement, calculated with the gain g averaged over the interval $t = 300$–600 ps, for the same pump pulse and T_e as in Fig. 4; the plasma parameters are $n_e = 3 \times 10^{19}$ cm^{-3}, $d = 0.1$ cm, $L = 5$ cm.

The experiments [74] confirmed the advantage of nanosecond pump pulses interacting with a cluster target along the plasma filament axis.

In summary, we will list the principal advantages of nanostructured targets.

(a) Almost complete suppression of pump pulse reflection or scattering and the absence of debris in the plasma.

(b) The possibility of obtaining optimal n_e, T_e, and d values throughout the plasma volume; the use of an axicon provides highly homogeneous plasma.

(c) Amplification occurs during a time interval of $\geqslant 500$ ps in a large volume ~ 0.03–0.05 cm^3 where the effect of plasma expansion might be negligible. We estimate the plasma expansion (with initial diameter of ~ 1 mm) with assumption that the temperature of the ion W XXIX does not exceed 100 eV: the experiments with porous targets [30–33] have proved that in general the ion temperature is about an order less than the electron temperature. The maximum ion velocity is $(200/m_i)^{1/2} \approx 10^6$ cm/c, where m_i is the mass of the ion W XXIX. Thus plasma expansion is less than 0.01 mm (less than 1%). Modifying the surface layer density in the initial target can compensate for the decrease in the plasma density near the surface.

(d) The possibility of self-focusing of amplified radiation using a conical target.

(e) The target might be fixed on a sharp tungsten tips to provide best isolation of the target.

For the development of the high-efficient new generation x-ray lasers it is necessary the accurate preliminary theoretical estimations of the porous target density and dimensions as well as time dependence of the function T_e. The calculations for the set of parameters n_e, $T_e(t)$, d are necessary to establish their optimal values. The product $gL \approx 14$ can be reached at $5 < L < 30$ cm: L must be chosen depending on the pumping source energy and experimental convenience for target operation and production. In order to minimize the effect of target expansion the diameter d must be chosen as large as possible with given pumping energy and axicon-optics parameters.

The experimental studies are necessary of the pumping pulse pedestal preceding the main (heating) pulse; its time duration and energy must be optimized. Similar studies were conducted in the earlier experiments with the solid targets using a prepulse. Note, that a steplike form of pumping pulse is preferable when using axicon, as the homogeneity of the plasma is achieved much faster than in the case of a Gaussian form of pulse intensity. On the other hand, when using steplike pulse there is no loss of plasma energy, inherent experiments using a prepulse.

Another problem is the adjustment of the diameter of the waveguide and the target, minimizing the loss of the pump beam on the axicon (outside the mirror area). Diffraction-free characteristic of Bessel beams have been founding applications in several fields of physics, mainly for harmonic generation [75]. There are no applications for x-ray laser production as it was suggested in Ref. [34]. The exception is the experiment [35] made for the gaseous targets. Also, there are no studies of Bessel beams interaction with nanostructured materials.

Heavy Pd-like ions are the most promising for creating high-efficiency quasicontinuous x-ray lasers based on the latest developments in the production of nanostructured materials as well as qualitatively new optical systems. They appear to be a basis for creating a new generation x-ray lasers.

Unfortunately, spectroscopic data for these ions are practically absent. The experimental transition energies in heavy Pd-like ions are needed to test the theoretical data to estimate the accuracy of calculations. Urgent problem is to study the spectra of Pd-like ions with $Z > 60$ with the use of plasma sources with low electron density.

[1] A. E. Bugrov *et al.*, JETP **84**, 497 (1997).
[2] T. H. Kuehl *et al.*, Hyperfine Interact. **162**, 55 (2005).
[3] O. L. Landen *et al.*, Eur. Phys. D **44**, 273 (2007).
[4] A. V. Vinogradov, I. I. Sobelman, and E. A. Yuokov, Sov. J. Quant. Electr. **5**, 59 (1975).
[5] D. L. Matthews *et al.*, Phys. Rev. Lett. **54**, 110 (1985).
[6] B. J. MacGowan, S. Maxon, P. L. Hagelstein, C. J. Keane, R. A. London, D. L. Matthews, M. D. Rosen, J. H. Scofield, and D. A. Whelan, Phys. Rev. Lett. **59**, 2157 (1987).
[7] K. A. Janulevicz, J. Tummler, G. Priebe, and P. V. Nickles, Phys. Rev. A **72**, 043825 (2005).
[8] J. Tummler, K. A. Janulewicz, G. Priebe, and P. V. Nickles, Phys. Rev. E **72**, 037401 (2005).
[9] A. Klisnick *et al.*, JOSA B- Opt. Phys. **17**, 1093 (2000).
[10] K. A. Janulewicz, A. Lucianetti, G. Priebe, W. Sandner, and P. V. Nickles, Phys. Rev. A **68**, 051802 (2003).
[11] K. A. Janulewicz, P. V. Nickles, R. E. King, and G. J. Pert, Phys. Rev. A **70**, 013804 (2004).
[12] H. T. Kim *et al.*, Phys. Rev. A **77**, 023807 (2008).
[13] S. Suckewer and P. Jaeglé, Laser Phys. Lett. **6**, 411 (2009).
[14] M. H. Mahdieh, R. Fazeli, and G. J. Talents, J. Phys. B: At. Mol. Opt Phys. **42**, 125602 (2009).
[15] C. Montcalm *et al.*, Opt. Lett. **19**, 1004 (1994).
[16] K. M. Skulina *et al.*, Appl. Opt. **34**, 3727 (1995).
[17] B. Sao-Lao and C. Montcalm, Opt. Lett. **26**, 468 (2001).
[18] A. E. Yakshin, I. V. Kozhevnikov, E. Zoethout, E. Louis, and F. Bijkerk, Opt. Express **18**, 6957 (2010).
[19] A. McPherson, B. J. Thompson, A. B. Borisov, K. Boyer, and C. K. Rhodes, Nature (London) **370**, 631 (1994).
[20] T. Ditmire, T. Donnelly, A. M. Rubenchik, R. W. Falcone, and M. D. Perry, Phys. Rev. A **53**, 3379 (1996).
[21] T. Ditmire *et al.*, Nature (London) **386**, 54 (1997).
[22] M. Lezius, S. Dobosz, D. Normand, and M. Schmidt, Phys. Rev. Lett. **80**, 261 (1998).
[23] M. A. Lebeault *et al.*, Eur. Phys. D **20**, 233 (2002).

[24] J. Zweiback, T. Ditmire, and M. D. Perry, Phys. Rev. A **59**, R3166 (1999).

[25] V. P. Krainov and M. B. Smirnov, Phys. Rep. **370**, 237 (2002).

[26] M. Mori *et al.*, J. Appl. Phys. **90**, 3595 (2001).

[27] S. Ter-Avetisyan, M. Schnurer, H. Stiel, U. Vogt, W. Radloff, W. Karpov, W. Sandner, and P. V. Nickles, Phys. Rev. E **64**, 036404 (2001).

[28] E. P. Ivanova and A. L. Ivanov, J. Exp. Theor. Phys. **100**, 844 (2005).

[29] E. P. Ivanova, N. A. Zinov'ev, and L. V. Knight, Quant. Electr. **31**, 683 (2001).

[30] I. N. Burdomsky, A. E. Bugrov, V. V. Gavrilov, A. Yu. Goltsov, N. G. Kovalsky, M. I. Pergament, and E. V. Zhuzhukalo, Rev. Sci. Instrum. **68**, 810 (1997).

[31] I. N. Burdonskiy *et al.*, J. Phys. IV **133**, 343 (2006).

[32] I. N. Burdonskiy *et al.*, J. Phys. IV **133**, 1001 (2006).

[33] N. G. Borisenko *et al.*, Laser Part. Beams **26**, 537 (2008).

[34] H. M. Milchberg, C. G. III. Durfee, and J. Lynch, J. Opt. Soc. Am. B **12**, 731 (1995).

[35] M.-C. Chou, P.-H. Lin, C.-A. Lin, J.-Y. Lin, J. Wang, and S.-Y. Chen, Phys. Rev. Lett. **99**, 063904 (2007).

[36] H.-H. Chu, H.-E. Tsai, M.-C. Chou, L.-S. Yang, J.-Y. Lin, C.-H. Lee, J. Wang, and S.-Y. Chen, Phys. Rev. A **71**, 061804(R) (2005).

[37] S. Sebban *et al.*, Phys. Rev. Lett. **86**, 3004 (2001).

[38] C. Chenais-Popovics, V. Malka, J.-C. Gathier, S. Gary, O. Peyrusse, M. Rabec-LeGloahec, I. Matsushima, C. Bauche-Arnoult, A. Bachelier, and J. Bauche, Phys. Rev. E **65**, 046418 (2002).

[39] E. P. Ivanova and L. V. Knight, J. X-ray Sci. Technol. **7**, 339 (1997).

[40] B. E. Lemoff, G. Y. Yin, C. L. Gordon III, C. P. J. Barty, and S. E. Harris, Phys. Rev. Lett. **74**, 1574 (1995).

[41] E. P. Ivanova and A. L. Ivanov, Quant. Electron. **34**, 1013 (2004).

[42] E. P. Ivanova, Optics Spectrosc. **94**, 151 (2003).

[43] E. P. Ivanova, Quant. Electron. **38**, 917 (2008).

[44] Y. Abou-Ali, A. Demir, G. J. Tallent, M. Edwards, R. E. King, and G. J. Pert, J. Phys B: At. Mol. Opt. Phys. **36**, 4097 (2003).

[45] P. D. Gasparyan, F. A. Starikov, and A. N. Starostin, Uspekhi Phiz. Nauk **41**, 761 (1998).

[46] A. Sureau and P. B. Holden, Phys. Rev. A **52**, 3110 (1995).

[47] O. Larroche, D. Ros, A. Klisnick, A. Sureau, C. Möller, and H. Guennou, Phys. Rev. A **62**, 043815 (2000).

[48] J. Zhang *et al.*, Science **276**, 1097 (1997).

[49] K. G. Whitney, A. Dasgupta, and P. E. Pulsifer, Phys. Rev. E **50**, 468 (1994).

[50] L. N. Ivanov, E. P. Ivanova, L. V. Knight, and A. G. Molchanov, Phys. Scr. **53**, 653 (1996).

[51] E. E. Fill, J. Quant. Spectrosc. Radiat. Transfer **39**, 489 (1988).

[52] N. A. Zinov'ev, Ph.D. thesis, Institute of Spectroscopy of Russian Academy of Sciences, 2002.

[53] J. Sugar and V. Kaufman, Phys. Scr. **26**, 419 (1982).

[54] Y. N. Joshi, Th. A. M. van Kleef, and C. G. Mahajan, J. Opt. Soc. Am. B **4**, 1306 (1987).

[55] S. S. Churulov, Y. N. Joshi, and A. N. Ryabtsev, J. Phys. B: At. Mol. Opt. Phys. **27**, 5485 (1994).

[56] S. S. Churilov, Y. N. Joshi, and A. N. Ryabtsev, Phys. Scr. **65**, 40 (2002).

[57] S. S. Churilov, A. N. Ryabtsev, W.-ÜL. Tchang-Brillet, and J.-F. Wyart, Phys. Scr. **61**, 420 (2000).

[58] S. S. Churilov, A. N. Ryabtsev, W.-ÜL. Tchang-Brillet, and J.-F. Wyart, Phys. Scr. **66**, 293 (2002).

[59] S. S. Churilov, A. N. Ryabtsev, W.-ÜL. Tchang-Brillet, J.-F. Wyart, and Y. N. Joshi, Phys. Scr. **71**, 589 (2005).

[60] J. Sugar, V. Kaufman, and W. L. Rowan, J. Opt. Soc. Am. B **10**, 799 (1993).

[61] L. N. Ivanov and L. I. Podobedova, J. Phys. B **10**, 1001 (1977).

[62] L. N. Ivanov and M. N. Driker, J. Phys. B **11**, 1695 (1978).

[63] E. P. Ivanova, Ph.D. thesis, Institute of Spectroscopy of Russian Academy of Sciences, 1992.

[64] E. P. Ivanova, L. N. Ivanov, A. V. Glushkov, and A. E. Kramida, Phys. Scripta **32**, 513 (1985).

[65] E. P. Ivanova and A. V. Gulov, At. Data Nucl. Data Tables **49**, 1 (1991).

[66] L. N. Ivanov, E. P. Ivanova, and L. V. Knight, Phys. Rev. A **48**, 4365 (1993).

[67] M. N. Driker and L. N. Ivanov, Opt. I Spektrosk. **49**, 209 (1980).

[68] M. N. Driker and L. N. Ivanov, Opt. I Spektrosk. **49**, 417 (1980).

[69] L. N. Ivanov, E. P. Ivanova, and L. V. Knight, Phys. Lett. A **206**, 89 (1995).

[70] E. P. Ivanova, Opt. Spectrosc. **103**, 733 (2007).

[71] E. P. Ivanova, At. Data Nucl. Data Tables **95**, 786 (2009).

[72] K. A. Janulevicz, P. V. Nickles, R. E. King, and G. J. Pert, Phys. Rev. A **70**, 013804 (2004).

[73] K. B. Kuntz, B. Braverman, S. H. Youn, M. Lobino, E. M. Pessina, and A. I. Lvovsky, Phys. Rev. A **79**, 043802 (2009).

[74] S. Ter-Avetisyan, U. Vogt, H. Stiel, M. Schnürer, I. Will, and P. V. Nickles, J. Appl. Phys. **94**, 5489 (2003).

[75] A. Averchi, D. Faccio, R. Berlasso, M. Kolesik, J. V. Moloney, A. Couairon, and P. Di Trapani, Phys. Rev. A **77**, 021802 (2008).